Agricultural Water Management 306 (2024) 109170

Contents lists available at ScienceDirect

Agricultural Water Management

journal homepage: www.elsevier.com/locate/agwat

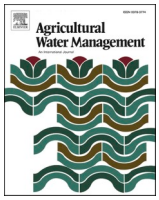

Biochar enhances soil hydrological function by improving the pore structure of saline soil

Angyuan Jia [a,b], Xiaojun Song [a], Shengping Li [a], Zhipeng Liu [c], Xiaotong Liu [d], Zixuan Han [a], Huizhou Gao [a], Qiqi Gao [a,b], Yan Zha [a], Ying Liu [b], Xueping Wu [a,*], Gang Wang [b,*]

[a] State Key Laboratory of Efficient Utilization of Arid and Semi-arid Arable Land in Northern China, the Institute of Agricultural Resources and Regional Planning, Chinese Academy of Agricultural Sciences, Beijing 100081, China
[b] College of Land Science and Technology, China Agricultural University, Beijing 100193, China
[c] College of Resources and Environmental Sciences, Nanjing Agricultural University, Nanjing 210095, China
[d] Institute of Resources and Environment, International Centre for Bamboo and Rattan, Key Laboratory of National Forestry and Grassland Administration/Beijing for Bamboo & Rattan Science and Technology, Beijing 100102, China

ARTICLE INFO

Handling Editor: Dr R Thompson

Keywords:
Biochar-amended soil
Least limiting water range
Soil aggregate stability
Soil pore characteristics
Soil water retention curve

ABSTRACT

The poor soil structure caused by salinization is a major factor affecting crop growth and soil structure will further affect hydrological function. Biochar is widely used to improve soil physical structure because of its special porous material. However, the mechanism of soil pore structure on hydrological function (e.g., soil saturated hydraulic conductivity, plant available water, least limiting water range) after biochar incorporation in saline soil remains unclear. Therefore, the present study examined the response of soil structural properties of different biochar addition in saline clay loam, and subsequently assessed how the pore structure influence soil hydrological function. The study involved four treatments: CK (Control)、C_1 (7.5 t ha^{-1} biochar)、C_2 (15 t ha^{-1} biochar)、C_3 (30 t ha^{-1} biochar). Soil aggregate stability increased from 15 % to 30 % when the amount of biochar addition increased from 7.5 t ha^{-1} to 30 t ha^{-1}. The highest connectivity index (2.36) and the highest fractal dimension (2.56) were found at the biochar addition of 30 t ha^{-1}. Biochar addition reduced the proportion of small pores (<50 μm pore size) at both soil depths of 0–10 cm and 10–20 cm, whereas increased the proportion of large pores (>300 μm pore size). Biochar amendment reduced the soil penetration resistance, with the soil saturated hydraulic conductivity, plant available water and the least limiting water range were measured 46 %, 27 % and 40 % greater in rate of 30 t ha^{-1} biochar addition as compared with those of the CK, respectively. Pearson's correlation analysis and redundancy analysis revealed that the soil saturated hydraulic conductivity was positively correlated with large pores (diameter >300 μm) and pore connectivity ($p < 0.05$). The lowest least limiting water range of the CK was primarily constrained by a relatively higher penetration resistance. The improved pore connectivity and elongated pore structures were the key responsible for the reduced penetration resistance in biochar-amended soil, which subsequently increased the least limiting water range. These quantitative estimates highlight the positive effects of biochar amendment-induced soil pore structure alternations towards improving soil hydrological functionalities. These findings are essential for devising effective strategies to enhance sustainable agriculture in saline soils.

1. Introduction

Soil salinization is the primary factor that contributes to global soil degradation and thus poses as a major threat to sustainable agricultural development (Singh, 2021). Saline lands show high salt content, sticky soil texture, poor infiltration capacity, and poor structural properties, leading to reduced crop yield (Li et al., 2014; Zhang et al., 2015). Poor soil structure is a critical factor that adversely affect the hydrological functions of saline soil. (He et al., 2014; Xu et al., 2021; Wang et al., 2022). Hence, optimizing soil structure and enhancing soil hydrological function are critical for improving the soil quality of saline lands (Castellini et al., 2015).

Biochar, an organic substitute, has been extensively utilized in recent years for improving the soil quality and the efficiency of salt leaching in

* Corresponding authors.
E-mail addresses: wuxueping@caas.cn (X. Wu), gangwang@cau.edu.cn (G. Wang).

https://doi.org/10.1016/j.agwat.2024.109170
Received 9 June 2024; Received in revised form 31 October 2024; Accepted 11 November 2024
Available online 16 November 2024

saline soils (Lee et al., 2022). Typically, biochar is a stable, carbon-rich by-product derived from biomass at high temperatures, it exhibits better stability and can serve as a long-term soil amendment agent as compared to other organic materials like straw, cow dung and commercial organic fertilisers (Fouladidorhani et al., 2024; Tejada et al., 2006; Yang et al., 2018;). Furthermore, the application of maize straw biochar increased the mean weight diameter (MWD) of soil aggregates (Pang et al., 2023), thereby altering the pore distribution characteristics and subsequently influencing the soil hydrological function of sandy loam soil (Chen et al., 2022).

The pore structure is a crucial parameter for the water transport and storage, air, and nutrients element in the soil matrix (Hernandez Gamboa et al., 2023). The traditional technique for determining the distribution of soil pore sizes relies on the soil water retention curve (SWRC). Amoakwah et al. (2017) reported that the application of 20 t ha^{-1} corn cob biochar notably improved soil water retention and increased microporosity (pore size < 3 μm) of sandy loam soil. The addition of 2 % mixture of rice husk, pine wood, and sugarcane bagasse biochar increased the proportion of soil macropores (pore size > 30 μm), which subsequently enhanced soil hydraulic conductivity in silt loam (Fouladidorhani et al., 2023). However, this method is not optimal for soils with larger pores and complex pore morphology. X-ray computed tomography is an effective approach to analyze soil pore structure, as it provides both visual representation and precise determination of valuable pore information. For example, by using this technique, more porous microstructure with connected pores can be seen in soils treated with biochar, and the improvement percentage increased significantly as the biochar application rate increases (He et al., 2020). However, a previous study has indicated that incorporating biochar into soil does not affect soil porosity, moreover, the addition of an unreasonable amount of biochar may have detrimental effects on soil pore structure determination by X-ray (Wang et al., 2023). Thus, examining the impact of biochar addition on soil pore morphology, which is helpful to understand the exploration of soil hydrology function.

Previous research has demonstrated that adding biochar to soil alters soil pore distribution, thereby affecting various parameters of soil hydrological function, including saturated water content (SWC), least limiting water range (LLWR), soil saturated hydraulic conductivity (K_S), field capacity (FC) and plant available water (PAW) (Li et al., 2020; Fouladidorhani et al., 2023). The SWC, FC, and PAW significantly increased following a short-term biochar treatment (Zhang et al., 2020). The PAW in soil amended with biochar is determined solely by the potential energy of soil water and does not take into account additional factors that may restrict plant water absorption (Tormena et al., 2017). LLWR represents the minimum water-limited range for plant growth, that is, the range within which crop growth is least restricted; LLWR is closely associated with soil water suction, aeration, and compaction. Some studies have confirmed that LLWR is a valuable gauge of soil physical health for supporting crop growth, and crop production shows a higher correlation with LLWR than with other soil structural properties (Benjamin and Karlen, 2014; Li et al., 2020). Biochar addition to soil affects soil compaction, water retention, and soil penetration resistance (Blanco-Canqui, 2017), thus has the potential to regulate LLWR in coarse soil (Saffari et al., 2021). The low LLWR induces an adverse effect on crop water utilization, impedes crop growth, and decreases crop production in clay soil. It is unclear whether the addition of biochar can affect the LLWR of saline soil. Hence, it is crucial to analyze the structural properties of biochar amended soils and hydrological function employing SWRC and CT scanning techniques.

It is critical to reveal the mechanism of soil pore structure regulating hydrologic function after biochar amendment in the coastal saline land. Hence, the purpose of this study: (i) examine the impact of biochar on soil pore structure characteristics based on CT examination; (ii) speculate and verify the impacts of varying levels of biochar incorporation on soil hydrological; and (iii) reveal the relationship between soil hydrological function and soil pore structure characteristics.

2. Materials and methods

2.1. Study area

The research was conducted in Dongying, a city in Shandong Province, China. The study area belongs to the National Technology Innovation Centre for Comprehensive Utilisation of Saline and Alkaline Land. This region has a temperate continental monsoon climate in the region (Fig. 1). The average annual temperature is 12.1°C, and the average annual rainfall varies from 500 to 600 mm. The precipitation during July and August contributes to around half of the total rainfall (Xia et al., 2019). The average annual evaporation rate is 1700–1800 mm. The experimental area was situated in a saline coastal land. The primary physicochemical characteristics of the experimental area soil are showed in Table 1.

2.2. Experimental design and materials

Based on the results of previous application of biochar on saline soil and the actual field application cost (Liang et al., 2021), the following biochar addition treatments were designed. Field plots (8 m × 5 m) were divided into four treatments in a randomized block design with three replicates each: (1) control with no biochar addition (CK); (2) biochar addition rate of 7.5 t ha^{-1} (C_1); (3) biochar addition rate of 15 t ha^{-1} (C_2); and (4) biochar addition rate of 30 t ha^{-1} (C_3). Biochar was produced from peanut shells at 500°C in Henan Provincial Biochar Engineering and Technology Research Centre, and specific properties of biochar were shown in Table 2. On May 10, 2022, biochar was evenly mixed into the surface soil of the test plots at a depth of 0–20 cm. Oil sunflower was chosen as the crop for the experiment, with a growth cycle of around 4 months. The fertilizer application rate was the same for all treatments (160 kg N ha^{-1}, 50 kg P ha^{-1}, and 60 kg K ha^{-1}).

2.3. Soil sample collection and analysis

2.3.1. Soil aggregate stability, bulk density, and scanning electron microscopy

Soil samples were collected from two different soil depths (0–10 cm and 10–20 cm) in September 2023 after harvesting oil sunflower. A total of nine core samples (100 cm^3) were collected from each plot to measure soil structural characteristics and hydrological properties. Soil saturated water conductivity was analyzed in the laboratory by collecting ring knives, which was determined through the constant head method with a 5 cm water column. Soil bulk density (BD) is measured after drying in an oven at 105°C degrees Celsius for 48 hours (Zhen et al., 2015). The calculation formula of soil total porosity (TP) is as follows:

$$TP = 1 - \frac{BD}{SD}$$

Where BD is bulk density (g cm^{-3}) and SD is soil density (2.65 g cm^{-3})

Soil aggregate stability was measured by a wet sieving method using sieves of the following sizes: 2000, 250, and 53 μm, followed by the calculation of mean weight diameter (MWD) and geometric mean diameter (GMD) of soil aggregates (Bach and Hofmockel, 2014). Scanning electron microscopy (SEM; SUPRA 55, Zeiss) was used to analyze the biochar and soil surface microstructure at a voltage of 5 kV for selected soil samples from each plot.

2.3.2. Soil water retention curve (SWRC)

The Kokusan H-1400PF centrifuge (Kokusan Corp; Tokyo) was used to measure SWRC, with the temperature maintained at 20°C throughout the measurement process. The 11 centrifugal speed levels were established based on matric potential values that range from 0 to 1500 kPa, with the following settings: 0, 300, 500, 800, 1300, 1800, 2400, 3300, 5400, 7700 and 9100 rpm. After each centrifuge comes to a stop at the

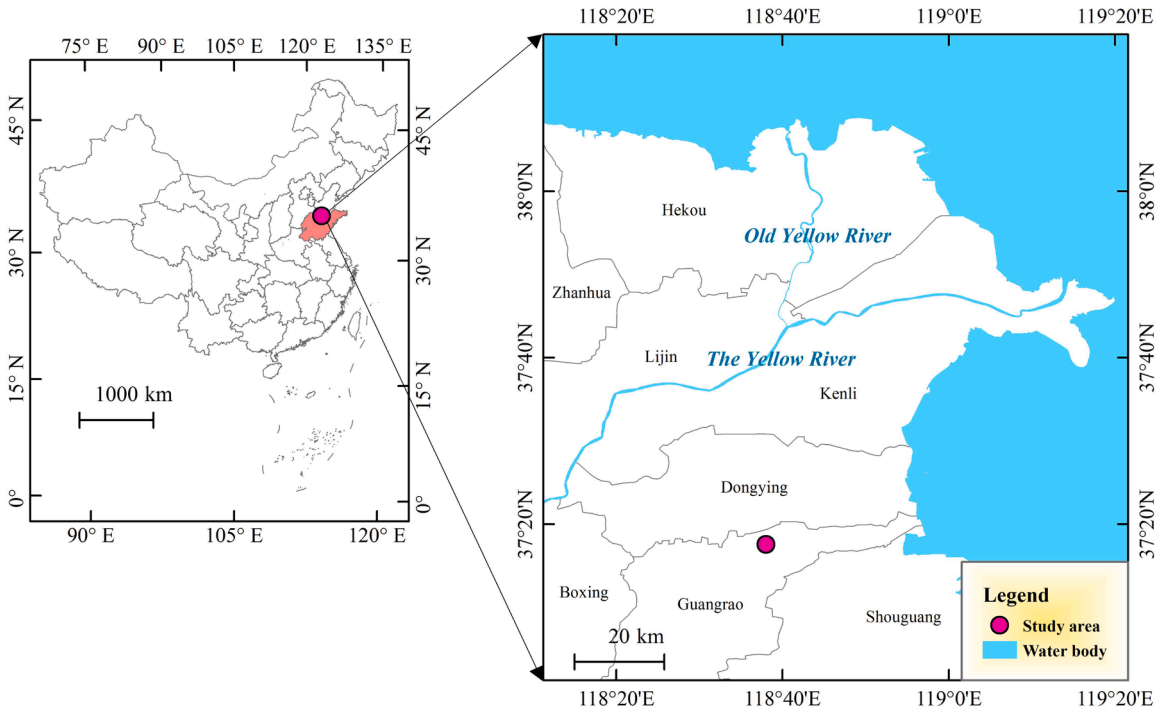

Fig. 1. The location of the experiment.

Table 1
The basic soil properties.

Soil depth (cm)	AK (mg kg^{-1})	SOC (g kg^{-1})	pH	EC (μs cm^{-1})	BD (g cm^{-3})	Sand %	Silt %	Clay %
0–20	90.10±5.31	7.81±1.04	8.93±0.17	1716±182	1.55±0.08	16.97±1.03	61.30±8.28	21.73±4.21
20–40	89.36 ±6.85	7.69±0.76	8.86±0.09	1714±156	1.54±0.1	15.33±1.27	60.73±6.71	23.9±3.52

Note: Values represent means followed by the standard deviation. AK, Available potassium; SOC, Soil organic carbon; BD, Bulk density; EC, Electric conductivity.

Table 2
The basic biochar properties.

	C	N	SA	BD	pH	Particle size (%)		
	(%)	(%)	(m^2 g^{-1})	(g cm^{-3})		1–2 mm	0.5–1 mm	<0.5 mm
Biochar	48±5	15±2	20±3	0.25±0.05	8.33±0.12	12.46±1.26	48.2±6.74	38.92 ±5.22

Note: Values represent means followed by the standard deviation. C, Soil organic carbon; N, Total nitrogen; SA, Specific surface area; BD, Bulk density

specified speed, the weight of the ring knife should be measured at that time. The experiment was set up with three replicate treatments and soil water content was analysed by taking the average of the three replicates. The soil moisture movement characteristics were determined by calibrating the centrifuge data with the van Genuchten model (van Genuchten, 1980):

$$\theta = (\theta_S - \theta_r)[1 + (ah)^n] + \theta_r$$

$$m = 1 - 1/n$$

The saturated volumetric water content is represented by θ_s (cm^3 cm^{-3}); while the residual volumetric water content is represented by θ_r (cm^3 cm^{-3}); and a, n, and m are fitting parameters.

2.3.3. CT scanning and image analysis

To analyze the soil pore structure, we scanned the 100 cm^3 samples using a CT scanning (Phoenix Nanotom S, GE, USA) at the Institute of Soil Science, Chinese Academy of Sciences, Nanjing. A total of 24 soil columns were collected from depths of 0–10 and 10–20 cm (Three biochar addition treatments and CK). The scanning parameters included a tube voltage of 100 kV, tube current of 100 A, and scanning resolution of 25 μm. Following the CT scanning process, a total of 2100 images were obtained from one soil column.

The software lmageJ (version 1.5eNIH, USA) was used to analyze the images. To mitigate the impact of the soil column's edge effect, a square region measuring 28 mm × 28 mm for diameter was chosen for subsequent image processing operations. Gaussian filtering is used to remove noise from the image. By comparing the binary image with the original greyscale image of the CT scan, the thresholds were visually adjusted. The ImageJ plug-in Analyze Particles was used to determine the pore number, pore surface area, and pore volume. The ImageJ plug-in Bone-J was used to evaluate fractal dimension and connectivity (Doube et al., 2010), the Euler characteristic was used to calculate connectivity density, the fractal dimension (FD) with the box counting method. The pore size distribution was classified into six levels according to the equivalent diameter: d < 50 μm, 50–100, 100–150, 150–200, and 200–300 μm; and

d > 300 μm (Peng et al., 2023). Pore shape factor (F) was categorized as regular (F ≥ 0.5), irregular (0.2 < F < 0.5), or elongated (F ≤ 0.2) (Zhou et al., 2012).

2.3.4. Penetration resistance (PR), and least limiting water range (LLWR)

Soil samples were collected from 0 to 10 cm and 10–20 cm using a ring knife (100 cm^3). Soil penetration resistance curves we obtained by measuring soil penetration resistance at different matric suctions (30, 100, 500, 1000, and 1200 kPa). The soil penetration resistance (PR) was measured using a micro-penetrometer (Omega LC703, USA, with a cone diameter of 2 mm) as outlined by Li et al. (2021). PR (MPa) was calculated as follows:

$$PR = aA^b$$

Where A is the soil moisture and *a* and *b* are the parameters used for fitting the model.

The water content was determined at an air-filled porosity (AFP) of 10 % using the following equation (Safadoust et al., 2014):

$$AFP = \left(1 - \frac{BD}{SD}\right) - 0.1$$

where BD is bulk density (g cm^{-3}) and SD is soil density (2.65 g cm^{-3})

LLWR and PAW was calculated by comparing the soil water content to the minimum thresholds of LLWR and PAW. The upper limit of LLWR ($LLWR_{up}$) and the lower limit of LLWR ($LLWR_{down}$) based on the method of (da Silva et al., 1994). The $LLWR_{up}$ was field capacity or at air-filled porosity of 10 %, whichever was the smaller. $LLWR_{down}$ was the permanent wilting point or at PR of 2 MPa, whichever was the higher.

2.4. Statistical analysis

A one-way ANOVA was performed to evaluate the influence of biochar addition, with significant differences considered at a probability level of 0.05. To explore the relationships between soil pore structure characteristics and hydrological function, pearson's correlation coefficients and redundancy analysis were employed. The statistical analysis was performed with the SPSS software (version 21, SPSS Inc.).

3. Results

3.1. Effects of biochar on soil aggregate distribution

The surface morphology of the original saline soil aggregates exhibited a dense and aligned structure in SEM image (Fig. 2b). Biochar addition for a single fertility period altered the surface morphology of soil aggregates (Fig. 2d). Specifically, biochar application formed large aggregates and increased soil aggregate stability in the 0–20 cm layer saline soil (Fig. 3). The construction of soil aggregates was impacted by the amount of biochar applied. The 30 t ha^{-1} biochar application treatment showed the highest proportion of >2 mm aggregates, which was 1.53-fold greater than that of CK (Fig. 3a), and the lowest proportion of <0.053 mm aggregates, which was 30 % lesser than that of CK. In the median (C_2) and highest (C_3) biochar application treatments, the GMD improved by 15–19 % and 25–30 % ($p < 0.05$, respectively) as compared to that of CK, whereas the lowest biochar application treatment (C_1) showed minimal changes in the GMD. A similar tendency was observed for the mean weight diameter (MWD) values across all treatments, with C_3 treatment showing a higher (26–40 %) value than CK (Fig. 3c).

3.2. Soil pore structure characteristics

Biochar addition altered soil pore morphology; long stripes of soil pore distribution and interconnected pore distribution were observed in C_3 treatment (Fig. 4). Based on the 3D reconstructed structure map of soil pores (0–20 cm), the soil pore particles in CK treatment were smaller than those in other three treatments; the soil pore volume increased as the amount of biochar application increased. Additionally, most of the pores in CK treatment were isolated, as evidenced by the decreased connectivity density. As biochar treatment amount increased from CK to C_3 treatment, tiny and isolated pores gradually developed and connected with each other to form larger pores.

Biochar addition altered the distribution of soil pore structure in

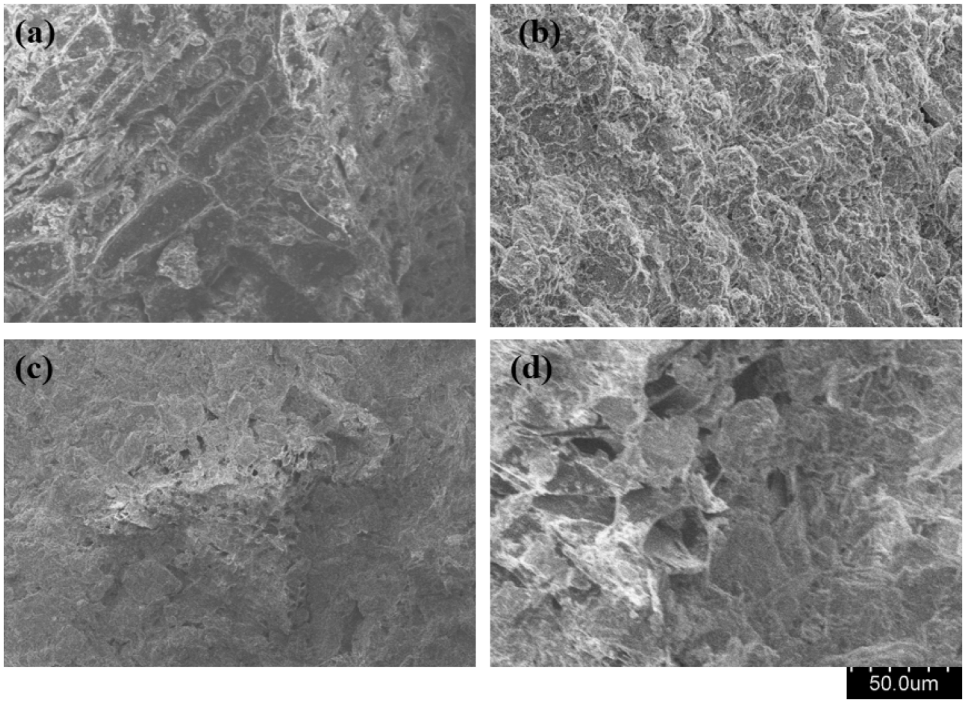

Fig. 2. The scanning electron microscope (SEM) images aggregate surface morphology, (a) Peanut shell biochar (b) original saline soil, (c) biochar-amended soil at 30 t ha^{-1}biochar (200 μm resolution) (d) biochar-amended soil at 30 t ha^{-1}biochar (50 μm resolution).

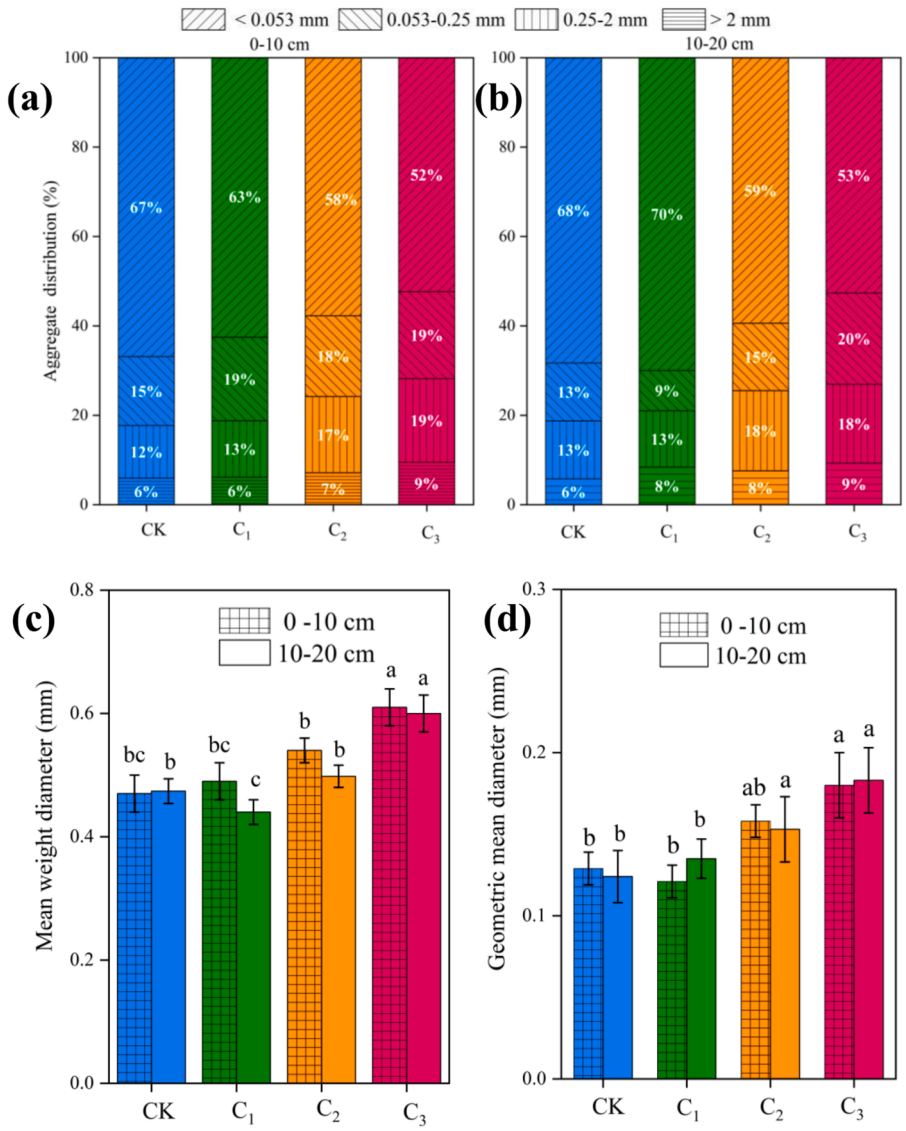

Fig. 3. The effect of biochar application on soil aggregate characteristics. (a) distribution of soil aggregates across various size fractions in 0–10 cm (b) distribution of soil aggregates across various size fractions in 10–20 cm (c) mean weight diameter in 0–10 cm, 10–20 cm (d) geometric mean diameter in 0–10 cm, 10–20 cm. CK (Control), C_1 (7.5 t ha^{-1}), C_2 (15 t ha^{-1}), and C_3 (30 t ha^{-1}). Note: Different lowercase letters indicate significant differences between the treatments at the 5 % level.

saline-alkali soil (Table 3). The porosity values of C_1, C_2, and C_3 treatments were greater by 8.2 %, 23 %, and 41.6 %, respectively, as compared to that of CK. C_3 showed the highest connectivity index (2.36) and the highest fractal dimension (2.56) compared to the other two biochar treatments. The percentage of pores with diameter < 50, 50–100, 100–150, 150–200, 200–300, and >300 μm contributed to 7 %, 23 %, 25 %, 13 %, 21 %, and 15 % of the total counted pores, respectively (Fig. 5). The CK treatment exhibited a significantly larger porosity (24–52 %) with pores of d < 50 μm than other treatments. Biochar addition decreased the number of small pores (d < 50 μm) at both soil depths but increased the proportion of larger pores (d > 300 μm), especially in C_3 treatment. Fig. 6 showed the distribution of pore shapes under different biochar addition treatments. The elongated pores accounted for >40 % of the total porosity in all treatments, and the proportion of elongated pores increased with the increase in biochar addition; in contrast, regular and irregular pores exhibited an opposite trend. Compared to CK, C_3 showed a significant increase in elongated pores by 30–38 % ($p < 0.05$).

3.3. Soil penetration resistance and soil bulk density

Fig. 7 showed the variations in soil penetration resistance. Soil penetration resistance decreased as the amount of biochar increased, the C_3 treatment showed a significant change compared with CK. The mean penetration resistance for the CK treatment were 21.5 % and 38.2 % higher than those for C_2 and C_3 respectively, there were also no significant differences between CK and C_1. CK exhibited the highest BD (Fig. 7c), and the total porosity of C_3 treatment compared to CK increased by 8.5 % and 8.9 % at the 0–10 cm and 10–20 cm, respectively.

3.4. Effect of biochar on soil hydrological function

Biochar application significantly affected the hydraulic characteristics of saline soil (Fig. 8; Table 4). The *Ks* showed a consistent upward trend as the amount of biochar increased (Table 4). The *Ks* value was significantly higher for biochar-treated soils than for CK, biochar addition (C_3) significantly increased the *Ks* by 46 % compared to the CK treatment ($p < 0.05$; Table 4). The comparison of FC across various

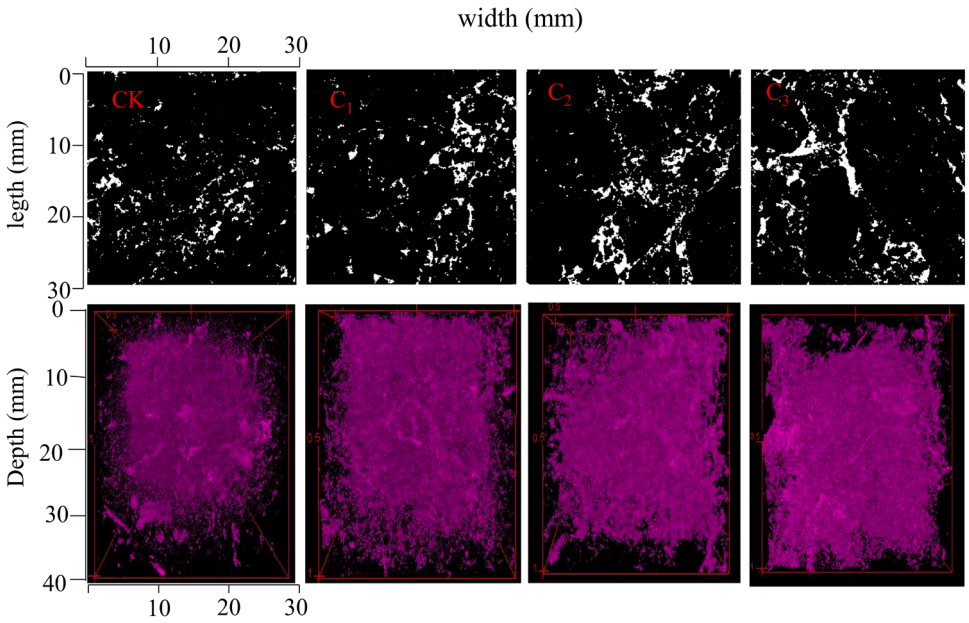

Fig. 4. The X-ray CT scanned 2D (up, 28 mm*28 mm) and 3D (low, 28 mm*28 mm*40 mm) images of soil cores upon biochar application. For the 2D images, white color represents soil pore distribution. CK (Control), C_1 (7.5 t ha^{-1}), C_2 (15 t ha^{-1}), and C_3 (30 t ha^{-1}).

Table 3
Soil pore structure characteristics by CT scanning.

	Soil depth (cm)	Soil porosity (%)	Pore number	Pore area (μm^2)	Anisotropy	Fractal dimension	Connectivity density
CK	0–10	2.71±0.21c	50809±8702b	14049±3620b	0.34±0.04a	2.31±0.21ab	1.88±0.34b
	10–20	2.75 ± 0.32c	67826±10245a	15059±2012ab	0.37±0.06a	2.07±0.13b	1.62±0.28c
C_1	0–10	2.91±0.25bc	49214± 9589b	15577± 3212b	0.31±0.05b	2.37±0.15b	1.69±0.21bc
	10–20	2.89±0.32b	60987±9002a	14788± 2006b	0.30±0.02b	2.21±0.15b	1.72±0.14bc
C_2	0–10	2.99±.21b	62634±10258a	16478±2537ab	0.34±0.03 a	2.31±0.21 a	1.88±0.15b
	10–20	3.13±0.57ab	51846±7355b	17323± 1556a	0.35±0.02a	2.53±0.19a	2.27±0.25ab
C_3	0–10	3.19±0.35a	78674±11254a	17444±1875a	0.38± 0.02a	2.55±0.25a	2.32±0.47a
	10–20	3.67±0.47a	58752±5526ab	18560±2856a	0.33±0.04ab	2.57±0.32 a	2.40±0.21a

Note: Values represent means followed by the standard deviation. Different letters indicate a significant difference among different biochar treatment at $p < 0.05$. Four treatments: CK (Control), C_1 (7.5 t ha^{-1}), C_2 (15 t ha^{-1}), and C_3 (30 t ha^{-1}).

biochar treatments revealed no significant difference between the C_1 treatment and CK; however, the FC value increased by 3 % in the 0–10 cm soil layer for C_3 treatment. The permanent wilting point (PWP) showed a lower value in all biochar treatments and decreased by 7 % in C_3 treatment ($p < 0.05$). The PAW values increased by 12 % and 25 % in C_2 and C_3 compared with CK, respectively. The LLWR value also showed an apparent increase with the increase in biochar application amount (Table 4). The C_1、C_2、C_3 treatment showed 9 %, 20 % and 35 % higher LLWR values than CK, respectively.

3.5. *The relationship between soil pore structure and hydrological function*

The correlation analysis between soil characteristics and hydrological function presented in Fig. 9. Significant positive correlations were found for *Ks* and connectivity density, pore size > 300 μm, fractal dimension ($p < 0.05$), while significant negative correlations existed between penetration resistance and *Ks* ($p < 0.05$). Additionally, significant positive correlations ($p < 0.05$) were found between PAW and pore area, fractal dimension. The correlations between elongated pore, connectivity density and LLWR were significantly positive ($p < 0.05$), while a negative correlation with penetration resistance ($p < 0.05$). These results confirmed that soil pore structure significantly influence soil hydrological function.

4. Discussion

4.1. *Effect of biochar addition on soil aggregate and pore structure*

Soil MWD and GMD are the critical indicators of soil aggregate stability and are used to characterize the resistance of soil aggregates to exogenous perturbations (Mustafa et al., 2020). In comparison with CK, the application of increasing amounts of biochar significantly enhanced MWD and GMD of saline soil (Fig. 3). The improvement of soil aggregate stability after biochar application might be due to the high carbon content of biochar and interact its interaction with microorganisms (Han et al., 2021; Ghorbani and Amirahmadi, 2024). Carbon molecules form chemical bonds with oxides, and organic matter becomes food for soil microbes, making the environment conducive to microbial growth (Rasul et al., 2022). Therefore, the soil microenvironment around biochar favored the development of microbial hotspots. Biochar has the potential to enhance the growth of fungal mycelia, increase the cohesion of soil particles, and facilitate its transformation into larger aggregates (Hammer et al., 2014; Zhang et al., 2024).

Biochar addition improved soil porosity and increased the proportion of pores with d > 50 μm in saline soil (Fig. 5). A previous study also reported a similar phenomenon, wherein biochar addition (1.5 t ha^{-1}) increased soil microporosity (d > 100 μm), fractal dimension, and connectivity index (16.6 %) as compared to CK (An et al., 2022). The

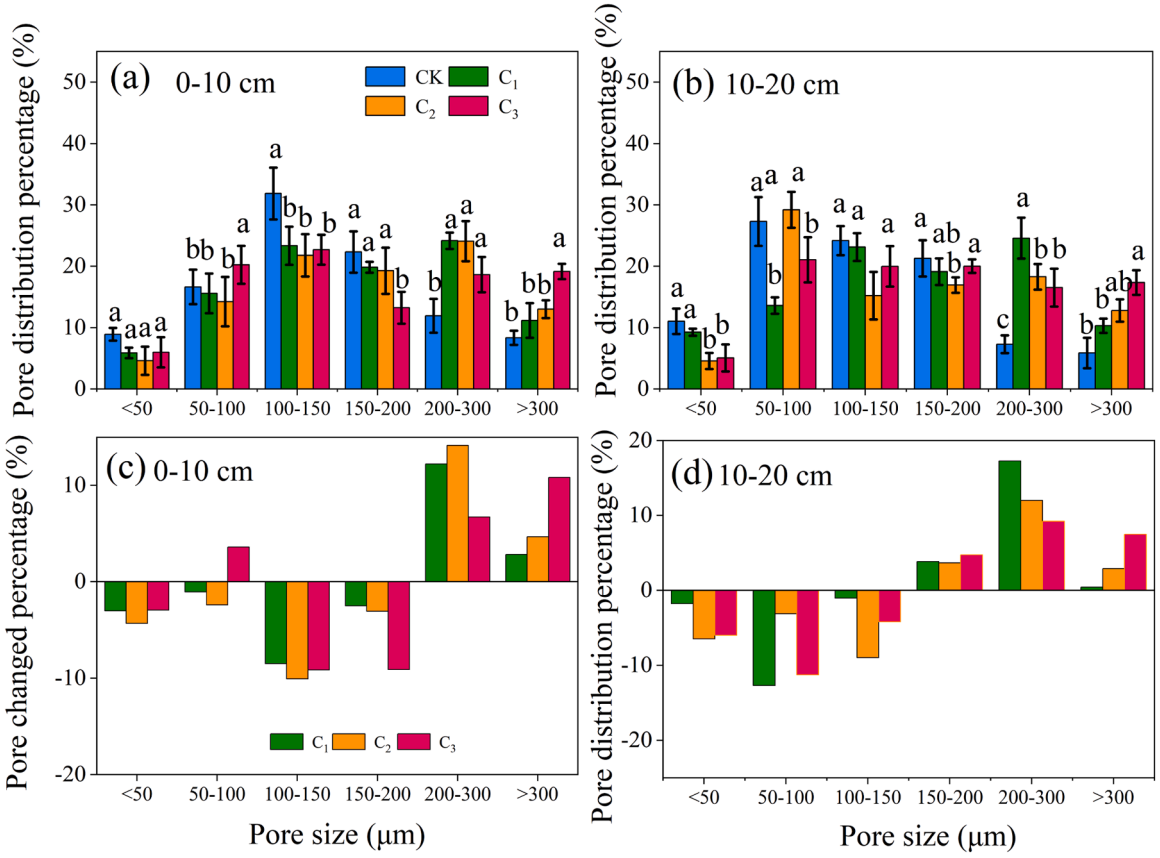

Fig. 5. Effect of biochar addition on soil pore size distribution. (a) soil pore size distribution in 0–10 cm; (b) soil pore size distribution in 10–20 cm; (c) Changes of different soil pore size after biochar addition in 0–10 cm (d) Changes of different soil pore size after biochar addition in 10–20 cm. CK (Control), C_1 (7.5 t ha^{-1}), C_2 (15 t ha^{-1}), and C_3 (30 t ha^{-1}). Different lowercase letters indicate significant differences between the treatments at the same soil depth at the 5 % level.

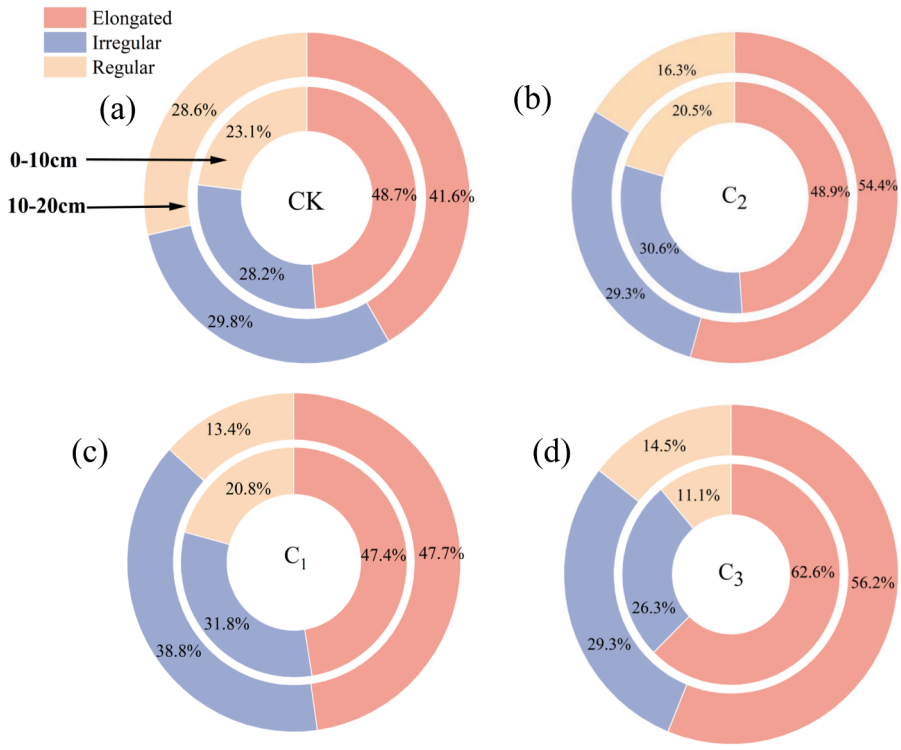

Fig. 6. Effect of biochar on soil pore shape distribution. Note: CK (Control), C_1 (7.5 t ha^{-1}), C_2 (15 t ha^{-1}), and C_3 (30 t ha^{-1}). (a) soil pore shape distribution of CK; (b) soil pore shape distribution of C_1 (c) soil pore shape distribution of C_2 (d) soil pore shape distribution of C_3.

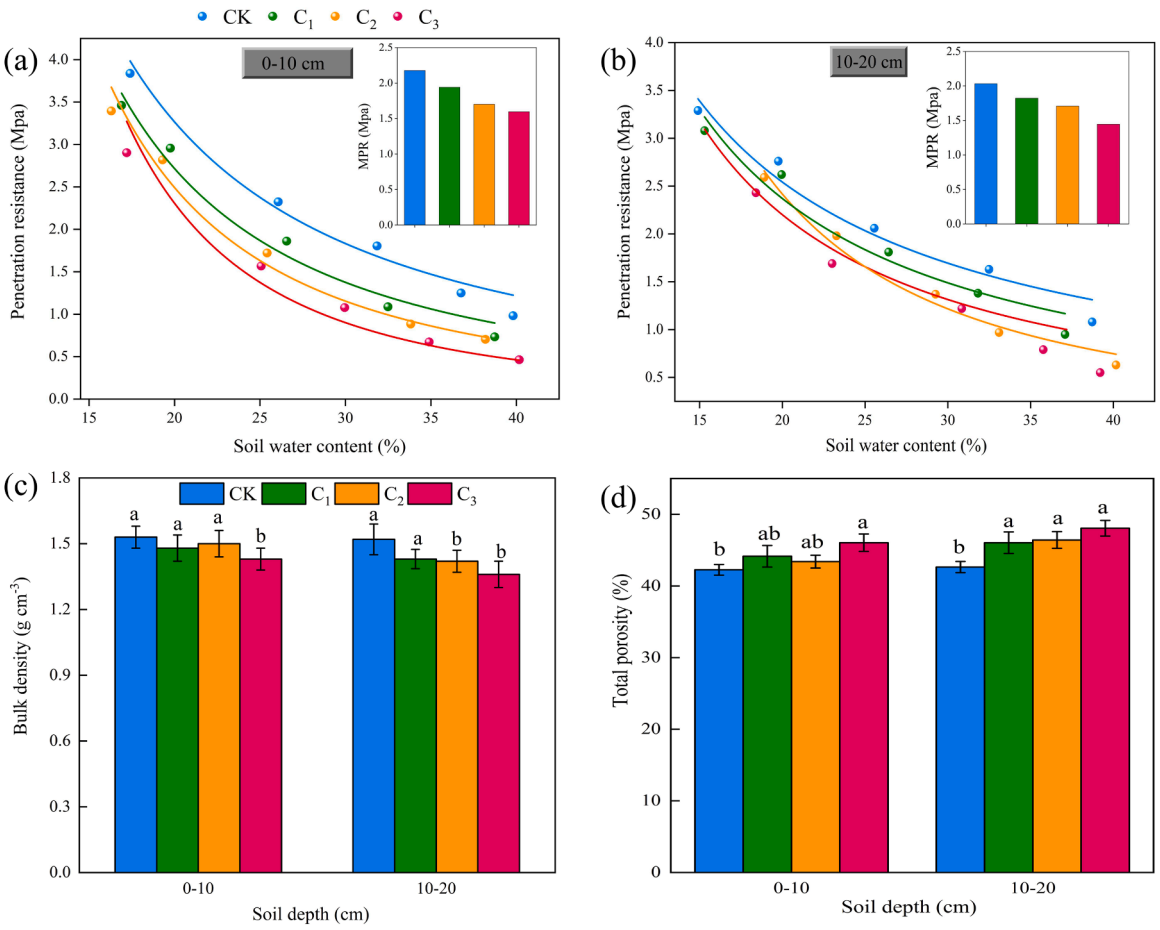

Fig. 7. Effect of biochar application on soil penetration resistance and bulk density. (a) change of soil penetration resistance with water content in 0–10 cm; (b) change of soil penetration resistance with water content in 10–20 cm; (c) soil density in 0–20 cm (d) soil total porosity in 0–20 cm MPR: mean penetration resistance. CK (Control), C_1 (7.5 t ha^{-1}), C_2 (15 t ha^{-1}), and C_3 (30 t ha^{-1}). Different lowercase letters indicate significant differences between the treatments at the same soil depth at the 5 % level.

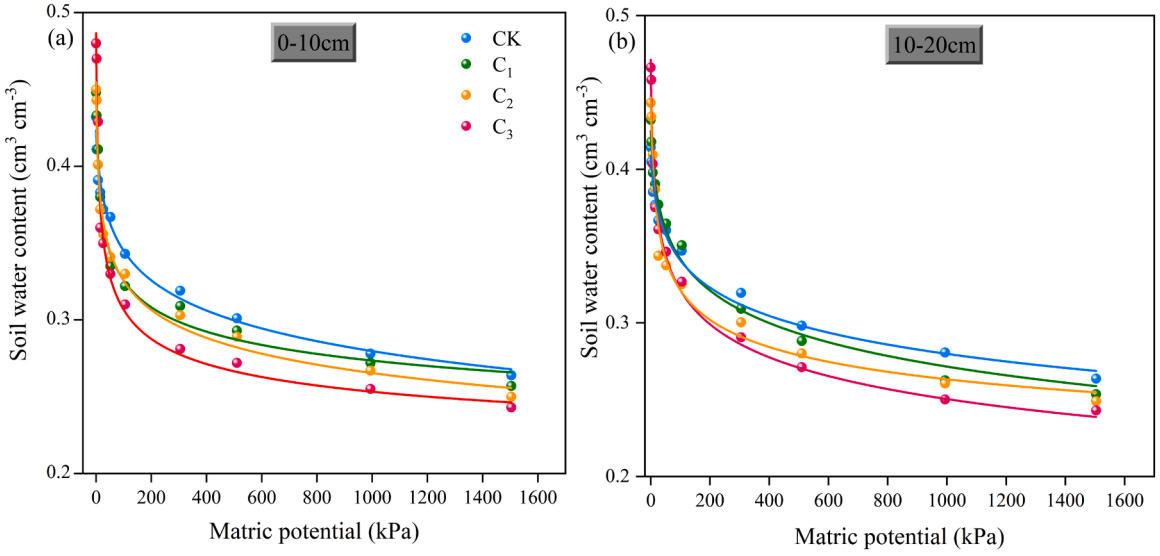

Fig. 8. Effect of biochar addition on soil water characteristic curve. Note: CK (Control), C_1 (7.5 t ha^{-1}), C_2 (15 t ha^{-1}), and C_3 (30 t ha^{-1}). (a) 0–10 cm soil water characteristic curve; (b) 10–20 cm soil water characteristic curve.

increase of microporosity was attributed to the increased organic carbon content following biochar addition (Yu et al., 2016). Biochar is a porous and rigid granular material, thus, it facilitates the enhancement of connectivity among the micropores within the soil (Faloye et al., 2024; Guo et al., 2021). Soil macroporosity (d > 300 μm) increased substantially during soil improvement following biochar addition, and the soil

Table 4
Soil hydrological function.

Layer (cm)	Index	CK	C_1	C_2	C_3
0–10	K_S (cm h^{-1})	0.21 ±0.02b	0.22 ±0.02b	0.26±0.02a	0.29± 0.03a
	FC (%)	37.18 ±2.28b	36.83 ±2.54 b	37.70 ±2.56b	38.12 ±2.36a
	PWP (%)	26.96 ±2.2a	26.68± 2.02a	25.93 ±1.21a	25.09 ±1.85b
	PAW (%)	10.22 ±0.74c	10.15 ±1.08c	11.77± 0.54b	13.03 ±1.21a
	AFP (%)	35.98 ±1.87a	35.60 ±1.51a	35.70 ±2.24a	36.50± 3.02a
	PR_2 (%)	27.86 ±1.35a	27.11 ±1.22a	25.98± 2.56b	23.71± 1.77c
	LLWR (%)	8.12± 1.02c	8.92 ±0.75bc	9.77± 1.23b	11.41 ±0.98a
10–20	K_S (cm h^{-1})	0.2± 0.03c	0.23± 0.02bc	0.25±0.03b	0.31 ±0.02a
	FC (%)	36.83± 1.03b	36.99 ±1.16b	37.76 ±0.87b	38.09 ±0.98a
	PWP (%)	26.85 ±1.35a	25.98± 0.87a	25.61± 1.02a	24.90 ±0.93b
	PAW (%)	9.98 ±1.23b	11.01 ±1.36b	12.15 ±1.02a	13.19 ±0.87a
	AFP (%)	35.92 ±2.02b	35.98 ±1.77b	35.65±0.94 b	36.76± 1.08a
	PR_2 (%)	27.50 ±2.51a	26.95 ±2.35a	24.59 ±2.01b	23.93 ±1.87c
	LLWR (%)	8.42 ±0.67b	9.03 ±0.59b	10.04 ±0.68ab	11.86 ±0.74a

Note: Values represent means followed by the standard deviation. Different letters indicate a significant difference among different biochar treatment at $p < 0.05$. K_S: soil saturated hydraulic conductivity ; FC: Field capacity; PWP: Permanent wilting point; PAW: Plant available water; AFP: air-filled porosity; PR_2: Soil water content in 2 Mpa penetration resistance; LLWR: Least limiting water range. CK (Control), C_1 (7.5 t ha^{-1}), C_2 (15 t ha^{-1}), and C_3 (30 t ha^{-1}).

pore structure evolved from a fine pore structure to a complex porous structure (Fig. 5). This is mainly due to the biochar contains a large number of pore structures that directly or indirectly create cracks and pores in the soil (Blanco-Canqui, 2017), while increasing the connectivity between small pores, resulting in an increase of soil pore diameter (Zhou et al., 2019). At the same time, the increase of fractal dimension of soil pores also indicates more well-developed developed soil structure soil structure (Table 3). Due to the high clay content and compact soil structure in the saline-alkali coastal land (Fig. 2), biochar mainly through expansion effect to optimize the soil pore structure (Wang et al., 2023; Sun et al., 2021).

More connected pores and biopore networks were observed by 3D visualization after biochar addition (Fig. 4). Thus, the formation of macropores by biochar addition plays a key role in promoting the elongated pore formation. Pre-existing macropores are preferentially selected and utilized by crop fine roots, which promotes an increase in crop fine root biomass and surface area and results in an in elongated pores (Abiven et al., 2015; Akpinar et al., 2023). Our results are supported by a significant positive correlation between the percentage of macropores and elongated pores (Fig. 9). The increase in the percentage of irregular and elongated pores (Fig. 6) facilitates water movement and solute transport in saline soil.

4.2. *The mechanism of soil pore structure regulating hydrological function in biochar-amended soil*

The soil hydrological function encompasses the capacity for water infiltration, water storage, and water conservation, which are the important indicator during the process of soil improvement and evaluation (Turunen et al., 2020). Soil saturated water conductivity increased with the increase of biochar application (Table 4), which aligns with the results in clay soil reported by Lim et al. (2016). The K_S exhibited a positive correlation with pores of diameter > 300 μm and connectivity density (Fig. 9). Even though large pores account only for a small part of soil pores, they play an essential role in soil water movement (Edeh and Mašek, 2022; Liu and Lu, 2023). Thus, the enhanced soil pore connectivity and macropore promotes the downward movement of water and facilitates water infiltration in saline soil (Pinto et al., 2023).

Biochar addition enriched soil pore structure and enhanced the surface area of soil pores, this improved the soil water holding capacity (Fig. 10). Biochar particles have internal pores that hold an additional amount of water, thereby increasing water retention following water addition to the soil (Adhikari et al., 2022). The soil water holding capacity was enhanced due to increase in the amount of soil storage pores following biochar addition (Yang et al., 2021). In the coastal saline soil, biochar increased the FC value by 3 % in C_3 treatment (Table 4). This is mainly due to the biochar is a distinctive soil enhancement agent, and most studies have shown positive the change in soil water storage capacity following biochar addition (Głąb et al., 2016; Abel et al., 2013). Consistent with our findings, the FC value significantly increased by

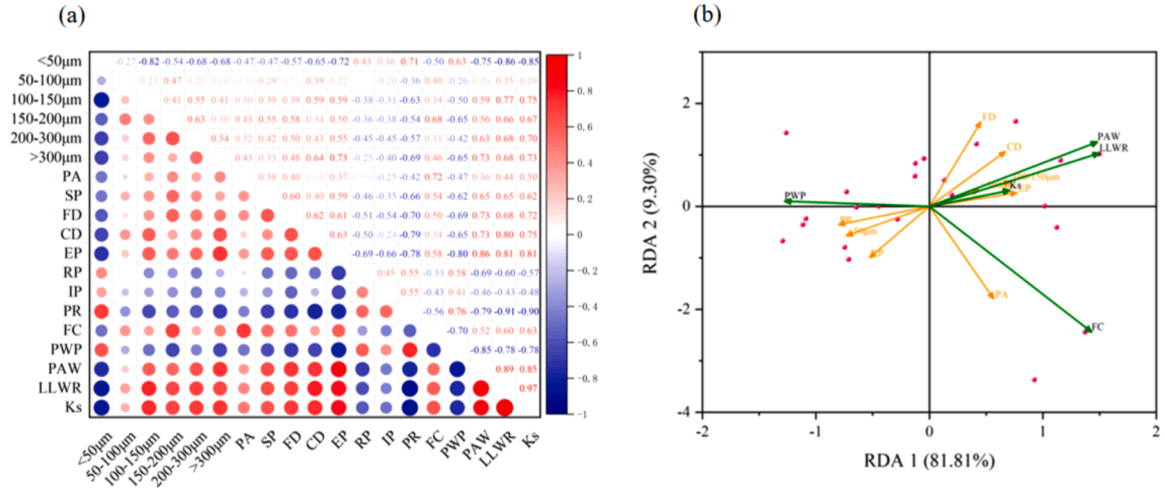

Fig. 9. Associations between soil hydrological function and pore structure. Note: (a) pearson's correlation between soil hydrological function and pore structure; (b) redundancy analysis. SP: Soil porosity by X-ray; FD: Fractal dimension; PA: Pore area; CD: Connectivity density; EP: Elongated pore; RP: Regular pore; IP: Irregular pore; PR: penetration resistance; FC: Field capacity; PAW: Plant available water; PWP: Permanent wilting point; LLWR: Least limiting water range; K_S: Soil saturated hydraulic conductivity; 50 μm, …, 300 μm are soil pore size.

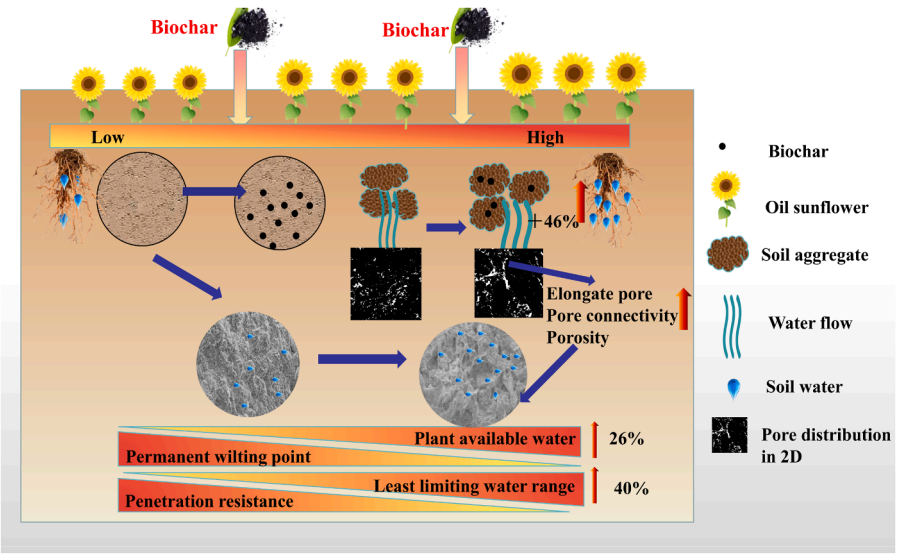

Fig. 10. Effect of biochar addition on soil pore structure and hydrological function concept map. For the pore 2D images, white color represents soil pore distribution; The grey substances are the SEM images of soil; Water flow represents saturated soil hydraulic conductivity; Elongate pore, pore connectivity, porosity represent soil pore structure characteristics.

4.4 % following wheat straw biochar treatment (applied at 1 % by weight) after a short incubation time in silt loam (Zhang et al., 2020). The PAW is determined based on FC and PWP, the rise of PAW (27 %) in C_3 treatment was primarily caused by the decrease in PWP (Table 4). The PAW has a positive correlation pore area and fractal dimension (Fig. 9), the enhancement of pore surface area and the fractal dimension of soil contribute to an increased capacity for soil water adsorption. In another study, forest waste biochar addition increases the specific surface area of the sand soil, which subsequently affects the soil structure and increases the PAW (Baiamonte et al., 2019).The addition of biochar as an organic binder enhances the aggregation of microaggregates into larger aggregates, thereby decrease the amount of micropores in the clay soil and enhance the formation of certain macropores (Liang et al., 2021; Islam et al., 2021). Thus, the reduction in the quantity of small and medium-sized pores in the soil decreases the permanent wilting point (Rahmati et al., 2019).The loose soil pore structure reduces the PWP after biochar addition (Table 4), which further increase the PAW of saline soil.

In comparison to other soil hydraulic properties, the LLWR serves as a comprehensive index that effectively reflects soil water retention capabilities, structural characteristics, and their implications for crop system (Safadoust et al., 2014). The LLWR increased 40 % at the high biochar addition treatment(30 t ha^{-1}) (Table 4), the larger amplitude of LLWR indicates that the soil is less susceptible to environmental pressures and improper aeration (Wilson et al., 2013). With the increase of biochar addition, $LLWR_{down}$ was determined from the water content at penetration resistance of 2 MPa (PR_2) to the permanent wilting point, this suggests that the inhibitory effect of soil penetration resistance on crop growth has been diminished. The investigation of the mechanisms through which biochar affects LLWR includes two main aspects: (1) the water absorption effect of biochar pores (Fig. 10), which is the primary reason for the increased water-holding capacity of the soil; (2) by changing the soil structure: the morphology of the improved soil pore structure affects soil compactness and aeration after adding corn residue biochar, thereby further influencing LLWR in a calcareous sandy loam soil (Blanco-Canqui, 2017; Saffari et al., 2021). The LLWR was positively correlated with soil pore fractal dimension, pore connectivity, and elongated pores ($p < 0.05$, Fig. 9). Accordingly, the increasing of elongated pores and soil pore structure connectivity contribute to the reduced saline soil penetration resistance, which is essential for enhancing least limiting water range. The increase of LLWR following the addition of biochar overcomes the challenges associated with crop water uptake, thereby improving crop water uptake and utilisation (de Moura et al., 2021). Taken together, our research validated that biochar has a beneficial impact on enhancing the soil hydrological function, and provide new insights into the soil pore structure regulating hydrological function following biochar addition in coastal saline land.

5. Conclusions

The present study revealed the characteristics of the soil pore structure, soil hydrological function, and their relationships in the coastal saline land. Biochar addition to saline soil significantly changed soil pore structure, which decreased the number of small pores ($d < 50$ μm) and increased the proportion of large pores ($d > 300$ μm). The high amount of biochar addition (30 t ha^{-1}) had the highest connectivity index, fractal dimension, soil porosity and elongated pores. The high amount of biochar addition changed the hydrological function of saline soil, reduced soil penetration resistance, and increased PAW and LLWR values; this facilitated and improved the absorption and proper utilization of water in the saline soil. Soil pore structure characteristics (connectivity index, elongated pore, and >300 μm porosity) are the important factors for LLWR increase in the saline soil. Furthermore, the determination of LLWR and soil pore structure characteristics by CT scanning is a suitable approach to evaluate soil structure and the hydrological function of saline soil following biochar treatment. These findings are essential for the sustainable development of biochar in enhancing and utilizing saline soils.

Author contributions

Angyuan Jia, Xueping Wu and Gang Wang conceived the research and designed the experiment. Angyuan Jia performed the experiments and data analyses and finished the initial manuscript. All authors analyzed and interpreted the data. All authors wrote the paper. All authors endorsed the final version of the document. Xueping Wu and Gang Wang initiated the project and coordinated it.

CRediT authorship contribution statement

Yan Zha: Investigation. **Ying Liu:** Validation, Supervision. **Xueping Wu:** Visualization, Resources, Funding acquisition. **Gang Wang:**

Resources, Funding acquisition, Conceptualization. **Angyuan Jia:** Writing – review & editing, Writing – original draft, Investigation, Funding acquisition, Formal analysis. **Xiaojun Song:** Software, Methodology, Data curation. **Shengping Li:** Validation, Formal analysis, Data curation. **Zhipeng Liu:** Methodology, Data curation. **Xiaotong Liu:** Supervision, Formal analysis. **Zixuan Han:** Validation, Methodology. **Huizhou Gao:** Validation, Investigation. **Qiqi Gao:** Visualization, Software.

Declaration of Competing Interest

The authors confirm that they do not have any conflicts of interest or personal relationships that could be perceived as affecting the conclusions presented in this paper.

Acknowledgments

This work was supported by the National Key Research and Development Program of China (2023YFD200140101, 2022YFD1500205), the Agricultural Science and Technology Innovation Program (ASTIP No. CAAS-ZDRW202407), the Pingduoduo-China Agricultural University Research Grant (PC2023B02007), the China Postdoctoral Science Foundation (2024T171020), and the open project of State Key Laboratory of Efficient Utilization of Arid and Semi-arid Arable Land in Northern China, the Institute of Agricultural Resources and Regional Planning, Chinese Academy of Agricultural Sciences (No. EUAL-2023–07).

Data availability

Data will be made available on request.

References

Abel, S., Peters, A., Trinks, S., Schonsky, H., Facklam, M., Wessolek, G., 2013. Impact of biochar and hydrochar addition on water retention and water repellency of sandy soil. Geoderma 202–203, 183–191. https://doi.org/10.1016/j.geoderma.2013.03.003.

Abiven, S., Hund, A., Martinsen, V., Cornelissen, G., 2015. Biochar amendment increases maize root surface areas and branching: a shovelomics study in Zambia. Plant Soil 395, 45–55. https://doi.org/10.1007/s11104-015-2533-2.

Adhikari, S., Timms, W., Mahmud, M.A.P., 2022. Optimising water holding capacity and hydrophobicity of biochar for soil amendment – A review. Sci. Total Environ. 851, 158043. https://doi.org/10.1016/j.scitotenv.2022.158043.

Akpinar, D., Tian, J., Shepherd, E., Imhoff, P.T., 2023. Impact of wood-derived biochar on the hydrologic performance of bioretention media: effects on aggregation, root growth, and water retention. J. Environ. Manag. 339, 117864. https://doi.org/10.1016/j.jenvman.2023.117864.

Amoakwah, E., Frimpong, K.A., Okae-Anti, D., Arthur, E., 2017. Soil water retention, air flow and pore structure characteristics after corn cob biochar application to a tropical sandy loam. Geoderma 307, 189–197. https://doi.org/10.1016/j.geoderma.2017.08.025.

An, N., Zhang, L., Liu, Y., Shen, S., Li, N., Wu, Z., Yang, J., Han, W., Han, X., 2022. Biochar application with reduced chemical fertilizers improves soil pore structure and rice productivity. Chemosphere 298. https://doi.org/10.1016/j.chemosphere.2022.134304.

Bach, E.M., Hofmockel, K.S., 2014. Soil aggregate isolation method affects measures of intra-aggregate extracellular enzyme activity. Soil Biol. Biochem. 69, 54–62. https://doi.org/10.1016/j.soilbio.2013.10.033.

Baiamonte, G., Crescimanno, G., Parrino, F., De Pasquale, C., 2019. Effect of biochar on the physical and structural properties of a desert sandy soil. Catena 175, 294–303. https://doi.org/10.1016/j.catena.2018.12.019.

Benjamin, J.G., Karlen, D.L., 2014. LLWR Techniques for quantifying potential soil compaction consequences of crop residue removal. Bioenerg. Res. 7, 468–480. https://doi.org/10.1007/s12155-013-9400-x.

Blanco-Canqui, H., 2017. Biochar and soil physical properties. Soil Sci. Soc. Am. J. 81, 687–711. https://doi.org/10.2136/sssaj2017.01.0017.

Castellini, M., Giglio, L., Niedda, M., Palumbo, A.D., Ventrella, D., 2015. Impact of biochar addition on the physical and hydraulic properties of a clay soil. Soil Tillage Res 154, 1–13. https://doi.org/10.1016/j.still.2015.06.016.

Chen, X., Duan, M., Zhou, B., Cui, L., 2022. Effects of biochar nanoparticles as a soil amendment on the structure and hydraulic characteristics of a sandy loam soil. Soil Use Manag 38, 836–849. https://doi.org/10.1111/sum.12740.

Doube, M., Klosowski, M.M., Arganda-Carreras, I., Cordelières, F.P., Dougherty, R.P., Jackson, J.S., Schmid, B., Hutchinson, J.R., Shefelbine, S.J., 2010. BoneJ: free and extensible bone image analysis in imageJ. Bone 47, 1076–1079. https://doi.org/10.1016/j.bone.2010.08.023.

Edeh, I.G., Mašek, O., 2022. The role of biochar particle size and hydrophobicity in improving soil hydraulic properties. Eur. J. Soil Sci. 73, 1–14. https://doi.org/10.1111/ejss.13138.

Faloye, O.T., Ajayi, E.A., Rostek, J., Schroeren, V., Babalola, T., Fashina, A., Horn, R., 2024. Hydraulic and pore functions of differently textured soils modified by biochar from different parts of the mango plant. Soil Tillage Res 236, 105944. https://doi.org/10.1016/j.still.2023.105944.

Fouladidorhani, M., Shayannejad, M., Mosaddeghi, M.R., Shariatmadari, H., Arthur, E., 2023. Biochar, manure and superabsorbent improve the physical quality of saline-sodic soil under greenhouse conditions. Soil Sci. Soc. Am. J. https://doi.org/10.1002/saj2.20538.

Fouladidorhani, M, Shayannejad, M, Shariatmadari, H., 2024. Pyrolysis of different organic feedstock combinations as soil amendments enhances the reclamation of saline-sodic soil. Soil Tillage Res 238, 105993. https://doi.org/10.1016/j.still.2023.105993.

van Genuchten, M.T., 1980. A closed-form equation for predicting the hydraulic conductivity of unsaturated soils. Soil Sci. Soc. Am. J. 44, 892–898. https://doi.org/10.2136/sssaj1980.03615995004400050002x.

Ghorbani, M., Amirahmadi, E., 2024. Insights into soil and biochar variations and their contribution to soil aggregate status – A meta-analysis. Soil Tillage Res 244, 106282. https://doi.org/10.1016/j.still.2024.106282.

Głąb, T., Palmowska, J., Zaleski, T., Gondek, K., 2016. Effect of biochar application on soil hydrological properties and physical quality of sandy soil. Geoderma 281, 11–20. https://doi.org/10.1016/j.geoderma.2016.06.028.

Guo, X. xia, Wu, S. biao, Wang, X. qing, Liu, H. tao, 2021. Impact of biochar addition on three-dimensional structural changes in aggregates associated with humus during swine manure composting. J. Clean. Prod. 280, 124380. https://doi.org/10.1016/j.jclepro.2020.124380.

Hammer, E.C., Balogh-Brunstad, Z., Jakobsen, I., Olsson, P.A., Stipp, S.L.S., Rillig, M.C., 2014. A mycorrhizal fungus grows on biochar and captures phosphorus from its surfaces. Soil Biol. Biochem. 77, 252–260. https://doi.org/10.1016/j.soilbio.2014.06.012.

Han, L., Zhang, B., Chen, L., Feng, Y., Yang, Y., Sun, K., 2021. Impact of biochar amendment on soil aggregation varied with incubation duration and biochar pyrolysis temperature. Biochar 3, 339–347. https://doi.org/10.1007/s42773-021-00097-z.

He, B., Cai, Y., Ran, W., Jiang, H., 2014. Spatial and seasonal variations of soil salinity following vegetation restoration in coastal saline land in eastern China. Catena 118, 147–153. https://doi.org/10.1016/j.catena.2014.02.007.

He, L., Zhao, J., Yang, S., Zhou, H., Wang, S., Zhao, X., Xing, G., 2020. Successive biochar amendment improves soil productivity and aggregate microstructure of a red soil in a five-year wheat-millet rotation pot trial. Geoderma 376, 114570. https://doi.org/10.1016/j.geoderma.2020.114570.

Hernandez Gamboa, C., Coutinho Figueiredo, G., Machado Vezzani, F., Carenhatto Ferreira, F., Bayer, C., 2023. Active plant biomass inputs influence pore system functioning in no-till soils. Geoderma 434 2023, 116477. https://doi.org/10.1016/j.geoderma.

Islam, M.U., Jiang, F., Guo, Z., Peng, X., 2021. Does biochar application improve soil aggregation? A meta-analysis. Soil Tillage Res 209, 104926. https://doi.org/10.1016/j.still.2020.104926.

Lee, X., Yang, F., Xing, Y., Huang, Y., Xu, L., Liu, Z., Holtzman, R., Kan, I., Li, Y., Zhang, L., Zhou, H., 2022. Use of biochar to manage soil salts and water: effects and mechanisms. Catena 211, 106018. https://doi.org/10.1016/j.catena. 2022.106018.

Li, J., Pu, L., Han, M., Zhu, M., Zhang, R., Xiang, Y., 2014. Soil salinization research in China: advances and prospects. J. Geogr. Sci. 24, 943–960. https://doi.org/10.1007/s11442-014-1130-2.

Li, S., Wu, X., Liang, G., Gao, L., Wang, B., Lu, J., Abdelrhman, A.A., Song, X., Zhang, M., Zheng, F., Degré, A., 2020. Is least limiting water range a useful indicator of the impact of tillage management on maize yield? Soil Tillage Res 199, 104602. https://doi.org/10.1016/j.still.2020.104602.

Liang, J., Li, Y., Si, B., Wang, Y., Chen, X., Wang, X., Chen, H., Wang, H., Zhang, F., Bai, Y., Biswas, A., 2021. Optimizing biochar application to improve soil physical and hydraulic properties in saline-alkali soils. Sci. Total Environ. 771. https://doi.org/10.1016/j.scitotenv.2020.144802.

Lim, T.J., Spokas, K.A., Feyereisen, G., Novak, J.M., 2016. Predicting the impact of biochar additions on soil hydraulic properties. Chemosphere 142, 136–144. https://doi.org/10.1016/j.chemosphere.2015.06.069.

Liu, J., Lu, S., 2023. Amendment of different biochars changed pore characteristics and permeability of Ultisol macroaggregates identified by X-ray computed tomography (CT). Geoderma 434, 116470. https://doi.org/10.1016/j.geoderma. 2023.116470.

de Moura, M.S., Silva, B.M., Mota, P.K., Borghi, E., Resende, A.V., de, Acuña-Guzman, S. F., Araújo, G.S.S., da Silva, L., de, C.M., de Oliveira, G.C., Curi, N., 2021. Soil management and diverse crop rotation can mitigate early-stage no-till compaction and improve least limiting water range in a Ferralsol. Agric. Water Manag. 243. https://doi.org/10.1016/j.agwat.2020.106523.

Mustafa, A., Minggang, X., Ali Shah, S.A., Abrar, M.M., Nan, S., Baoren, W., Zejiang, C., Saeed, Q., Naveed, M., Mehmood, K., Núñez-Delgado, A., 2020. Soil aggregation and soil aggregate stability regulate organic carbon and nitrogen storage in a red soil of southern China. J. Environ. Manag. 270. https://doi.org/10.1016/j.jenvman.2020.110894.

Pang, J., Wang, Y., Wang, B., Wang, J., Liu, E., Gao, F., Sun, S., Ren, X., Jia, Z., Wei, T., Zhang, P., 2023. Biochar application increases maize yield under film mulching due to higher soil organic content and soil aggregate stability in a semi-arid area. J. Soils Sediment. 23, 1718–1732. https://doi.org/10.1007/s11368-023-03444-8.

Peng, J., Yang, Q.S., Zhang, C.Y., Ni, S., Wang, J., Cai, C., 2023. Aggregate pore structure, stability characteristics, and biochemical properties induced by different cultivation durations in the Mollisol region of Northeast China. Soil Tillage Res 233, 105797. https://doi.org/10.1016/j.still.2023.105797.

Pinto, U., Rao, S., Phillip Svozil, D., Wright, A., Goonetilleke, A., 2023. Understanding the role of land use for urban stormwater management in coastal waterways. Water Res 245, 120658. https://doi.org/10.1016/j.watres.2023.120658.

Rasul, M., Cho, J., Shin, H.S., Hur, J., 2022. Biochar-induced priming effects in soil via modifying the status of soil organic matter and microflora: a review. Sci. Total Environ. 805, 150304. https://doi.org/10.1016/j.scitotenv.2021.150304.

Safadoust, A., Feizee, P., Mahboubi, A.A., Gharabaghi, B., Mosaddeghi, M.R., Ahrens, B., 2014. Least limiting water range as affected by soil texture and cropping system. Agric. Water Manag. 136, 34–41. https://doi.org/10.1016/j.agwat.2014.01.007.

Saffari, N., Hajabbasi, M.A., Shirani, H., Mosaddeghi, M.R., Owens, G., 2021. Influence of corn residue biochar on water retention and penetration resistance in a calcareous sandy loam soil. Geoderma 383, 114734. https://doi.org/10.1016/j.geoderma.2020.114734.

da Silva, A.P., Kay, B.D., Perfect, E., 1994. Characterization of the least limiting water range of soils. Soil Sci. Soc. Am. J. 58, 1775–1781. https://doi.org/10.2136/sssaj1994.03615995005800060028x.

Singh, A., 2021. Soil salinization management for sustainable development: a review. J. Environ. Manag. 277, 111383. https://doi.org/10.1016/j.jenvman.2020.111383.

Sun, X., She, D., Fei, Y., Wang, H., Gao, L., 2021. Three-dimensional fractal characteristics of soil pore structure and their relationships with hydraulic parameters in biochar-amended saline soil. Soil Tillage Res 205, 104809. https://doi.org/10.1016/j.still.2020.104809.

Tejada, M., Garcia, C., Gonzalez, J.L., Hernandez, M.T., 2006. Use of organic amendment as a strategy for saline soil remediation: influence on the physical, chemical and biological properties of soil. Soil Biol. Biochem. 38, 1413–1421. https://doi.org/10.1016/j.soilbio.2005.10.017.

Tormena, C.A., Karlen, D.L., Logsdon, S., Cherubin, M.R., 2017. Corn stover harvest and tillage impacts on near-surface soil physical quality. Soil Tillage Res 166, 122–130. https://doi.org/10.1016/j.still.2016.09.015.

Turunen, M., Hyväluoma, J., Heikkinen, J., Keskinen, R., Kaseva, J., Hannula, M., Rasa, K., 2020. Quantifying the pore structure of different biochars and their impacts on the water retention properties of Sphagnum moss growing media. Biosyst. Eng. 191, 96–106. https://doi.org/10.1016/j.biosystemseng.2020.01.006.

Wang, S., Gao, P., Zhang, Q., Shi, Y., Guo, X., Lv, Q., Wu, W., Zhang, X., Li, M., Meng, Q., 2022. Application of biochar and organic fertilizer to saline- alkali soil in the Yellow River Delta: effects on soil water, salinity, nutrients, and maize yield. Soil Use Manag 38, 1679–1692. https://doi.org/10.1111/sum.12829.

Wang, L., Luo, P., Jiang, C., Shen, J., Liu, F., Xiao, R., Wu, J., 2023. Distinct effects of biochar addition on soil macropore characteristics at different depths in a double-rice paddy field. Sci. Total Environ. 857, 159368., 10.1016/j.scitotenv.2022.159368.

Wilson, M.G., Sasal, M.C., Caviglia, O.P., 2013. Critical bulk density for a Mollisol and a Vertisol using least limiting water range: effect on early wheat growth. Geoderma 192, 354–361. https://doi.org/10.1016/j.geoderma.2012.05.021.

Xia, J., Ren, J., Zhang, S., Wang, Y., Fang, Y., 2019. Forest and grass composite patterns improve the soil quality in the coastal saline-alkali land of the Yellow River Delta, China. Geoderma 349, 25–35. https://doi.org/10.1016/j.geoderma.2019.04.032.

Xu, W., Li, K., Chen, L., Kong, W., Liu, C., 2021. The impacts of freeze–thaw cycles on saturated hydraulic conductivity and microstructure of saline–alkali soils. Sci. Rep. 11, 1–15. https://doi.org/10.1038/s41598-021-98208-0.

Yang, L., Bian, X., Yang, R., Zhou, C., Tang, B., 2018. Assessment of organic amendments for improving coastal saline soil. L. Degrad. Dev. 29, 3204–3211. https://doi.org/10.1002/ldr.3027.

Yang, C., Liu, J., Lu, S., 2021. Pyrolysis temperature affects pore characteristics of rice straw and canola stalk biochars and biochar-amended soils. Geoderma 397, 115097. https://doi.org/10.1016/j.geoderma.2021.115097.

Yu, X., Wu, C., Fu, Y., Brookes, P.C., Lu, S., 2016. Three-dimensional pore structure and carbon distribution of macroaggregates in biochar-amended soil. Eur. J. Soil Sci. 67, 109–120. https://doi.org/10.1111/ejss.12305.

Zhang, M., Song, X., Wu, X., Zheng, F., Li, S., Zhuang, Y., Man, X., Degré, A., 2024. Microbial regulation of aggregate stability and carbon sequestration under long-term conservation tillage and nitrogen application. Sustain. Prod. Consum. 44, 74–86. https://doi.org/10.1016/j.spc.2023.11.022.

Zhang, T., Wang, T., Liu, K.S., Wang, L., Wang, K., Zhou, Y., 2015. Effects of different amendments for the reclamation of coastal saline soil on soil nutrient dynamics and electrical conductivity responses. Agric. Water Manag. 159, 115–122. https://doi.org/10.1016/j.agwat.2015.06.002.

Zhang, Y., Yang, J., Yao, R., Wang, X., Xie, W., 2020. Short-term effects of biochar and gypsum on soil hydraulic properties and sodicity in a saline-alkali soil. Pedosphere 30, 694–702. https://doi.org/10.1016/S1002-0160(18)60051-7.

Zhen, Q., Ma, W., Li, M., He, H., Zhang, X., Wang, Y., 2015. Effects of vegetation and physicochemical properties on solute transport in reclaimed soil at an opencast coal mine site on the Loess Plateau, China. Catena 133, 403–411. https://doi.org/10.1016/j.catena.2015.06.009.

Zhou, H., Peng, X., Peth, S., Xiao, T.Q., 2012. Effects of vegetation restoration on soil aggregate microstructure quantified with synchrotron-based micro-computed tomography. Soil Tillage Res. 124, 17–23. https://doi.org/10.1016/j.still.2012.04.006.